ResearchGate

See discussions, stats, and author profiles for this publication at: https://www.researchgate.net/publication/273485778

Signature Vibrational Bands for Defects in CVD Single Layer Graphene by Surface Enhanced Raman Spectroscopy

ARTICLE *in* JOURNAL OF PHYSICAL CHEMISTRY LETTERS · FEBRUARY 2015

Impact Factor: 7.46 · DOI: 10.1021/jz5027272

CITATION
1

READS
41

4 AUTHORS:

Dallas Matz
The University of Arizona
10 PUBLICATIONS **20** CITATIONS
SEE PROFILE

Hossein Sojoudi
Massachusetts Institute of Technology
22 PUBLICATIONS **556** CITATIONS
SEE PROFILE

Samuel Graham
Georgia Institute of Technology
147 PUBLICATIONS **2,139** CITATIONS
SEE PROFILE

Jeanne E Pemberton
The University of Arizona
175 PUBLICATIONS **4,724** CITATIONS
SEE PROFILE

Available from: Dallas Matz
Retrieved on: 29 January 2016

THE JOURNAL OF PHYSICAL CHEMISTRY Letters

Letter

pubs.acs.org/JPCL

Signature Vibrational Bands for Defects in CVD Single-Layer Graphene by Surface-Enhanced Raman Spectroscopy

Dallas L. Matz,[†] Hossein Sojoudi,[‡] Samuel Graham,[‡] and Jeanne E. Pemberton*[,†]

[†]Department of Chemistry and Biochemistry, University of Arizona, 1306 East University Boulevard, Tucson, Arizona 85721, United States

[‡]George W. Woodruff School of Mechanical Engineering, Georgia Institute of Technology, 801 Ferst Drive, Atlanta, Georgia 30332, United States

Supporting Information

ABSTRACT: We report the observation of signature vibrational bands in the frequency region between 900 and 1600 cm^{-1} for defects in single-layer graphene (SLG) using surface Raman spectroscopy in ultrahigh vacuum. Vapor deposition of Ag leads to the formation of surface nanoparticles that migrate to defects in the SLG, leading to surface-enhanced Raman scattering (SERS) of the graphene G and 2D bands as well as new vibrational modes ascribed to native defects. Many of the new spectral bands of these native defects are similar, although not identical, to those predicted previously for $-C_2$ defects. These new bands are observed in addition to bands more commonly observed for defective graphene that are attributed to the D, G*, D+G, and 2D′ modes. The defects observed in these SLG films are not believed to result from the Ag deposition process but are postulated to be formed during the graphene CVD growth process. These defects are then made visible by postdeposition of Ag due to SERS.

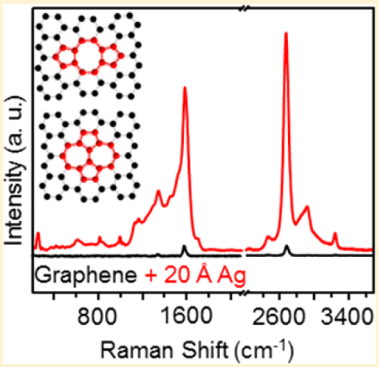

The synthesis of graphene via chemical vapor deposition (CVD) on transition metals such as Ru,[1] Ir,[2] Ni,[3] and Cu,[4] provides a cost-effective method for producing high-quality graphene on a large scale with lengths up to 100 m by roll-to-roll processing.[5] These advances in production have propelled interest in technological applications of graphene that require large-scale synthesis to fabricate devices such as transparent electrodes, sensors, and transistors. However, for broad use and optimizing its potential in various applications, its chemical and physical attributes, including the nature of structural defects introduced during the CVD growth and transfer processes, must be understood.

Raman spectroscopy is a method widely used to characterize graphene because the spectrum is highly sensitive to a multitude of changes in graphene characteristics. Raman spectroscopy is useful in providing insight into the effects of doping,[6−16] structural defects,[17−20] edge chirality,[21,22] uni- and biaxial strain,[23−25] pressure, and temperature[11,26] and most commonly as a measure of the number and quality of graphene layers.[27−30] The Raman spectrum of pristine SLG is characterized by two bands: the G band at ∼1585 cm^{-1}, from in-plane longitudinal vibrations of sp^2-hybridized C−C bonds, and the 2D band at ∼2700 cm^{-1} due to double-resonance intervalley dispersion involving two phonons with opposite momenta.[18,27,28,30] Careful monitoring of the frequency, line width, shape, intensity, and intensity ratio of the 2D to G bands [I(2D)/I(G)] can provide valuable information about graphene physiochemical properties.[18,27,30,31]

Two additional spectral features are occasionally observed in the pristine graphene spectrum near 1350 and 2450 cm^{-1} corresponding to the D and G* bands, respectively; both are bands induced by disorder.[17−20] The D band arises from ring breathing vibrations of sp^2 C atoms, and the G* band results from intervalley electron−phonon scattering similar to the 2D band but with one electron−phonon scattering event of slightly lower energy due to the presence of defects.[17,29,32,33]

Defects in the hexagonal lattice of graphene due to atomic deficiencies or rearrangement have been reported on the basis of both experimental (electron microscopy[34−36]) and computational investigations (density functional theory, DFT[34,37,38]). These structural defects have in common rearrangement of the graphene lattice resulting most commonly in the existence of pentagons (5), heptagons (7), octagons (8), and in rare cases nonagons (9). These rings combine to make localized networks of nonhexagonal rings and are often cataloged by the sequential listing of numbered rings, for example, 5−9 for the pentagon−nonagon structure that results from the removal of one carbon atom. A more complete examination of the multitude of combinations possible can be found in recent review articles.[34,39] The two most common of these defects are the Stone−Wales (SW) and the C_2 deletion ($-C_2$).

The SW defect has been predicted by theory[40−46] and experimentally observed in high-resolution (HR) TEM experiments[35,36,47−49] of various sp^2 carbon systems (graphene,

Received: December 26, 2014
Accepted: February 16, 2015
Published: February 16, 2015

ACS Publications © 2015 American Chemical Society

DOI: 10.1021/jz5027272
J. Phys. Chem. Lett. 2015, 6, 964−969

single-wall nanotubes, and C_{60}), although its experimental vibrational spectrum has not been reported. The SW defect forms by rotation of two adjacent carbon atoms by 90°, resulting in transformation of four adjacent hexagons (6−6−6−6) into a pentagon−heptagon−heptagon−pentagon (5−7−7−5) ring structure. The $-C_2$ defect occurs as the result of the deletion of two adjacent carbon atoms, leaving a hole; this defect results in a pentagon−octagon−pentagon (5−8−5) ring structure as opposed to the four hexagon ring structure of native graphene.[34] Figure 1 shows comparative structures for

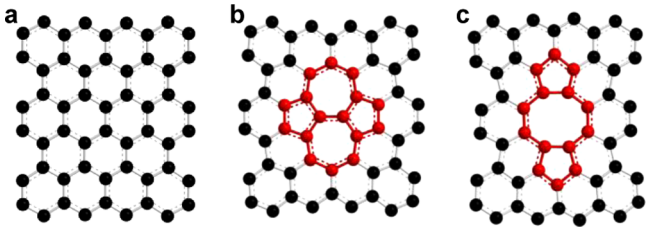

Figure 1. Molecular structures of (a) perfect graphene, (b) Stone−Wales defect, and (c) the $-C_2$ vacancy. The nonhexagonal rings that occur as a result of defect formation are depicted in red.

pristine graphene and graphene with SW and $-C_2$ defects, respectively. The $-C_2$ structure has also been observed with HR TEM[35,36,48] and STM[50] and has been predicted by theory.[43,50−52]

Previous studies in this laboratory and others have shown that vapor deposited Ag on organic films under vacuum conditions results in surface-enhanced Raman scattering (SERS) through the formation of Ag nanoparticles on the organic surface.[53−56] Thus, Ag deposition can be employed as a method for SERS of thin films such as graphene. Toward this end, the goal of this work was to use SERS to explore the physiochemical nature of solution-transferred CVD graphene. The results of this study are expected to provide important insight into the possible use of CVD single-layer graphene (SLG) in organic electronic devices.

In this work, SLG was grown via CVD on Cu foil following the procedures outlined previously by Li et al.[4] The SLG sheets, protected by a poly(methyl methacrylate) (PMMA) overlayer, were then transferred using a solution-based process to polished polycrystalline Ag substrates, which serve as reflective, inert substrates. The solution-transfer process entails oxidative removal of the growth substrate (thin Cu foil) in dilute aqueous $FeCl_3$ overnight, capture of the resulting floating PMMA/SLG assembly on a chemically polished Ag substrate, followed by removal of the PMMA protective coating by washes in anisole (1 h), warm acetone (1 h @ 50 °C), ethanol (three times), and finally nanopure water (two times). The Ag substrates, chemically polished using procedures previously reported from this laboratory,[57,58] have been shown to be clean and devoid of carbonaceous contamination[58] and only weakly enhancing (enhancement factors ∼10−30) due to their low surface roughness (∼1 nm rms roughness by AFM.)[59] SLG-on-Ag substrates are then transferred into the load-lock antechamber of a custom built ultrahigh vacuum system for thin-film Ag deposition and Raman spectral acquisition while remaining isolated from atmosphere.[56,60] Further details regarding the experimental procedures and materials can be found in the Supporting Information.

Figure 2 shows Raman spectra of a pristine SLG sheet before (black) and after deposition of 0.5 (blue), 1.0 (green), 1.5 (gold), and 2.0 (red) nm of Ag. Spectra were collected by coaddition of 120 spectra, each with a 5 s integration time, using 532 nm excitation at a power of 25−30 mW in ultrahigh vacuum. The spectrum before Ag deposition shows only the G and 2D bands at 1580 and 2690 cm^{-1}, respectively, characteristic of SLG. However, upon deposition of Ag, an increase in overall intensity of 20−60 times is observed, consistent with surface enhancement from nucleation of Ag nanoparticles on the graphene surface. In addition to surface enhancement of the G and 2D bands, multiple new bands evolve with increasing Ag coverage. The most prominent of these new spectral features is the asymmetric envelope of bands on the low-frequency side of the G band from 1100 to 1580 cm^{-1}. It is likely that the origin of some of this spectral broadening is due to the presence of amorphous carbon (a-C) from slight degradation of the film, as it has been well-documented that an asymmetric broadening of both the G and D bands occurs upon amorphization.[33,61,62] However, in addition to the emergence of a-C, four discrete bands at 1121, 1160, 1339, and 1446 cm^{-1} are clearly distinguishable superimposed on top of this broad envelope. In addition, a significant new discrete band at 250 cm^{-1} is clearly observed.

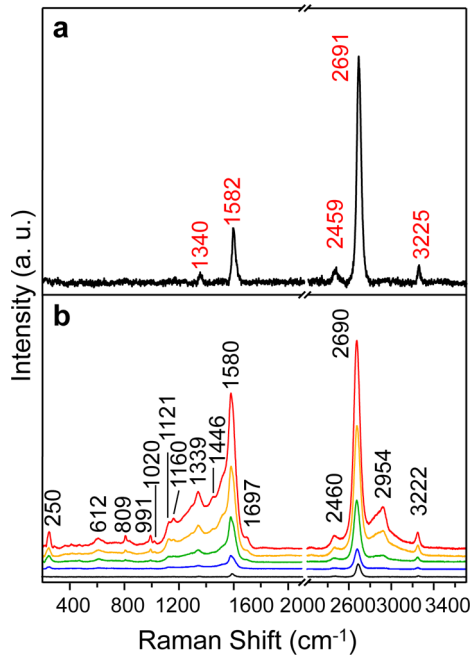

Figure 2. (a) Raman spectrum of CVD SLG and (b) Raman spectra of a graphene monolayer before (black) and after deposition of 0.5 (blue), 1.0 (green), 1.5 (gold), and 2.0 (red) nm of Ag.

The morphology of thin metal films on graphene has been studied by scanning tunneling microscopy (STM)[63−66] and transmission electron microscopy (TEM)[67,68] on suspended graphene as well as by both DFT[69,70] and first-principles calculations.[71] Clusters or nanoparticles are formed on graphene for Al,[67,70] Fe,[68−70] Pd,[63,67] Co,[63,68] Rh,[63] Pt,[63,71] Ti,[67,71] Au,[67,69] Cr,[67] Ni,[67] and Mo.[68] Several previous studies have shown using SEM that vacuum deposition of 2−5 nm thick films of Ag on graphene result in the formation of islands on the order of 15−25 nm in size depending on temperature and changes induced by annealing.[64−66] Zhou et al.[63] have shown that the size of these metal clusters is metal-dependent and correlated to the metal cohesion energy, with Pt and Rh forming clusters of ∼2−5 nm dia and Pd and Co forming

DOI: 10.1021/jz5027272
J. Phys. Chem. Lett. 2015, 6, 964−969

slightly larger clusters of ∼10−15 nm diameter Both theoretical and experimental results are consistent with cluster formation at graphene lattice defect sites at which dangling sp^2 bonds and distortion of the graphene π-electron system facilitate metal coordination.[63,68−70,72]

The Raman signal enhancement observed is attributed to SERS from formation of Ag nanoparticles on the graphene surface that, if their size and the excitation wavelength are appropriately matched, provide electric field enhancement through excitation of localized surface plasmons.[73] The results observed here are similar to those reported previously by Zhou et al. for thermal deposition of 2 nm of Ag onto SLG.[64] However, although they observed similar asymmetric broadening to the low-frequency side of the G band and the appearance of D, G*, D+G, and 2D′ bands, their spectra did not exhibit the additional discrete bands shown in the spectra in Figure 2. Zhou et al. further report that upon annealing a 5 nm thick Ag film, an average Ag nanoparticle size of ∼50 nm results based on postdeposition SEM images, although no mention of graphene structural changes that might lead to new vibrational bands is made. Moreover, these researchers report an overall enhancement of ∼50 in the Raman intensity, similar to the enhancement observed in the spectra in Figure 2. Although the spectra observed in this work and the previous report by Zhou et al. are similar, one difference in methodology is worth noting. The SLG used in this work is CVD graphene, which produces high-quality continuous sheets of ∼1.5 × 1.5 cm^2, whereas Zhou utilized mechanically exfoliated graphene from graphite.

One concern for the current study may be the influence of residual PMMA, used as a protective layer for transfer of CVD SLG, on the observed Raman spectra. Previous SERS studies have utilized PMMA as a flexible support for both graphene and metal nanoparticles due to its transparency and low Raman activity. This previous work uniformly documents little interfering Raman spectral signal from PMMA,[74−76] therefore precluding trace PMMA as the source of any of the observed signals in this work.

As previously noted, a number of nonhexagonal defect structures in SLG have been reported; however, there is little known about the specific Raman vibrational signatures of individual defects. To date, the Raman vibrational frequencies of only the two most common of these graphene defects, the SW and $-C_2$, have been reported by Kudin et al., as calculated using DFT.[77] The bands predicted for the $-C_2$ defects exhibit considerable similarity, both in frequency and relative intensity, to the new bands observed upon Ag deposition. For comparison, Figure 3 shows the spectrum of SLG after deposition of 2.0 nm of Ag (black) overlaid with bars representing both the frequencies and relative intensities of the calculated $-C_2$ and SW defect spectra.[77]

In previous HR TEM studies of graphene defects, the defects were created by bombardment with ∼100 keV beams of electrons with a flux of 60,000 electrons/nm^2, allowing the rearrangements and deletions to occur by overcoming the 5−8 eV barrier to defect formation.[37,78] This large barrier makes the formation of these defects by thermal deposition of metal atoms, as in the experiments reported here, unlikely. In fact, these defects are only likely to form under extreme nonequilibrium conditions such as high-energy flux (i.e., HR TEM experiments) or at temperatures in excess of 1300 K, such as might be experienced during CVD growth. On this basis, it is proposed that the defects observed here in the Raman spectra after Ag deposition are artifacts of graphene film growth,

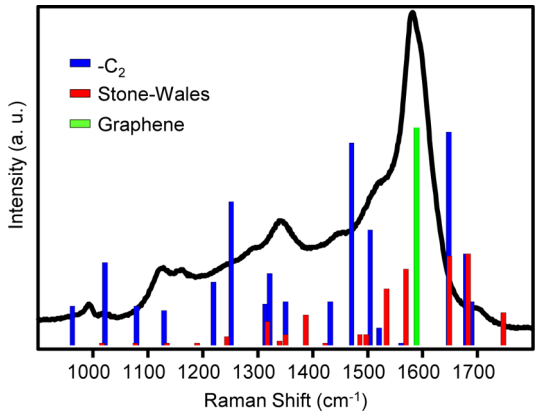

Figure 3. Raman spectra of a graphene monolayer after deposition of 2.0 nm of Ag (black) overlaid on the simulated frequencies for Stone−Wales (red bars) and $-C_2$ (blue bars) defects as well as the G band of graphene (green bar). Simulated spectral frequencies and relative intensities from ref 77.

existing in the SLG films prior to Ag deposition, but then made visible by SERS from deposited Ag nanoparticles. It is further noted that due to the high energy barrier for defect formation in what is assumed to be an activated process, it is unlikely that the defects would reorganize back to graphene at room temperature, thereby allowing their observation in these experiments.[34] Further support for the existence of defects in the SLG films prior to metal deposition is shown in Figure S1 of the Supporting Information; these spectra are from different SLG films after transfer to Ag substrates and placed into the UHV environment. Bands attributable to defects are weak in intensity but distinguishable in some of these spectra prior to Ag deposition. Nonetheless, given the known catalytic activity for trench formation on various forms of graphene by Ag nanoparticles,[79,80] the possibility that defects are formed at room temperature by exposure to the Ag nanoparticles in the presence of the 532 nm laser excitation cannot be ruled out.

Defect sites are proposed to be selectively enhanced by preferential segregation of Ag nanoparticles to these lower energy surface sites. DFT calculations by Lim et al.[70] indicate a strong preference for coordination of Fe and Al nanoparticles by graphene defects due to strong hybridization between the nanoparticles and dangling sp^2 bonds. Similar preferential coordination of Ag nanoparticles at defects is further supported by the observation of a new band at 250 cm^{-1}, which is assigned to a δ(C−Ag−C) mode and is supported by the normal coordinate analysis and DFT calculations of Stanghellini.[81]

The vibrational spectra for both the $-C_2$ and SW defects calculated by Kudin et al.[77] using DFT exhibit bands across a similar range of frequencies between ∼900 and 1600 cm^{-1} on the low-energy side of the G band as observed here (Figure 3). The calculated spectra also show similar distribution of intensities, with the general trend of higher intensities at higher frequencies and lower intensities for lower frequency bands.

One significant difference between the predicted vibrational response and the results observed here can be seen on the high-frequency side of the G band. Specifically, the $-C_2$ vacancy is predicted to have vibrational bands in this region at 1647, 1676, and 1686 cm^{-1}, and the SW defect is predicted to have bands at 1645, 1680, and 1744 cm^{-1}. However, very little vibrational activity is observed in this frequency region in the SLG

DOI: 10.1021/jz5027272
J. Phys. Chem. Lett. 2015, 6, 964−969

spectrum shown in Figure 3. Table 1 shows a comparison of the calculated frequencies reported by Kudin et al. and those

Table 1. Observed and Calculated Peak Frequencies for $-C_2$ and SW Defects

frequencies			
	calculated[a]		
+ 20 Å Ag observed	$-C_2$	Stone−Wales	assignments[b]
250			ν(C−Ag−C)
612			
809			
991	961		
1020	1020		
	1077		
1121	1125		
1160			
	1220		
	1250		
	1311	1316	
	1320		
1339	1350	1350	D-band
1446	1429		
	1467		
		1482	
	1502	1496	
1519	1516	1531	
		1565	
1580			G-band
	1647	1645	
	1676	1680	
1697	1686		
		1744	
2460			G*-band
2690			2D-band
2954			D+G′-band
3222			2D′-band

[a]Predicted frequencies from ref 77. [b]Assignments from ref 82.

observed in the spectra in Figure 1. Those frequencies listed near 1700 cm^{-1} are attributable to carbon atoms that are shared between five- and six-membered rings.[77] On the basis of the lack of any observable peaks above 1700 cm^{-1}, as would be expected for SW defects, we tentatively conclude that $-C_2$ defects are more prevalent and indeed may be the predominant defect type present in these films. However, it should be recognized that preferential aggregation of Ag nanoparticles at the $-C_2$ defects through coordination, as supported by the observation of the δ(C−Ag−C) band near 250 cm^{-1}, may give rise to preferential enhancement of only the $-C_2$ defects, even when SW defects are present. Thus, one must be cautious in eliminating the presence of specific defects on the basis of these spectra. Nonetheless, the data support the assertion that defects similar in chemical structure to the $-C_2$ defects are likely to be present in these SLG films based on the new spectral peaks that are observed between 900 and 1600 cm^{-1} after deposition of Ag.

■ ASSOCIATED CONTENT

Supporting Information

Additional experimental details of CVD graphene preparation, thin-film Ag deposition, and surface Raman spectroscopy. Additional spectra of pristine SLG films are also provided. This material is available free of charge via the Internet at http://pubs.acs.org.

■ AUTHOR INFORMATION

Corresponding Author

*E-mail: pembertn@u.arizona.edu.

Notes

The authors declare no competing financial interest.

■ ACKNOWLEDGMENTS

These studies were supported as part of the Center for Interface Science: Solar Electric Materials, an Energy Frontier Research Center funded by the U.S. Department of Energy, Office of Science, Office of Basic Energy Sciences, under award number DE-SC0001084.

■ REFERENCES

(1) Sutter, P. W.; Flege, J.-I.; Sutter, E. A. Epitaxial Graphene on Ruthenium. *Nat. Mater.* **2008**, *7*, 406−411.

(2) Coraux, J.; ÑDiaye, A. T.; Busse, C.; Michely, T. Structural Coherency of Graphene on Ir(111). *Nano Lett.* **2008**, *8*, 565−570.

(3) Reina, A.; Jia, X.; Ho, J.; Nezich, D.; Son, H.; Bulovic, V.; Dresselhaus, M. S.; Kong, J. Large Area Few-Layer Graphene Films on Arbitrary Substrates by Chemical Vapor Deposition. *Nano Lett.* **2008**, *9*, 30−35.

(4) Li, X.; Cai, W.; An, J.; Kim, S.; Nah, J.; Yang, D.; Piner, R.; Velamakanni, A.; Jung, I.; Tutuc, E.; et al. Large-Area Synthesis of High-Quality and Uniform Graphene Films on Copper Foils. *Science* **2009**, *324*, 1312−1314.

(5) Kobayashi, T.; Bando, M.; Kimura, N.; Shimizu, K.; Kadono, K.; Umezu, N.; Miyahara, K.; Hayazaki, S.; Nagai, S.; Mizuguchi, Y.; et al. Production of a 100-M-Long High-Quality Graphene Transparent Conductive Film by Roll-to-Roll Chemical Vapor Deposition and Transfer Process. *Appl. Phys. Lett.* **2013**, *102*, 023112.

(6) Graf, D.; Molitor, F.; Ensslin, K.; Stampfer, C.; Jungen, A.; Hierold, C.; Wirtz, L. Spatially Resolved Raman Spectroscopy of Single- and Few-Layer Graphene. *Nano Lett.* **2007**, *7*, 238−242.

(7) Berciaud, S. p.; Ryu, S.; Brus, L. E.; Heinz, T. F. Probing the Intrinsic Properties of Exfoliated Graphene: Raman Spectroscopy of Free-Standing Monolayers. *Nano Lett.* **2008**, *9*, 346−352.

(8) Yoon, D.; Moon, H.; Son, Y.-W.; Choi, J. S.; Park, B. H.; Cha, Y. H.; Kim, Y. D.; Cheong, H. Interference Effect on Raman Spectrum of Graphene on SiO_2/Si. *Phys. Rev. B* **2009**, *80*, 125422.

(9) Casiraghi, C.; Pisana, S.; Novoselov, K. S.; Geim, A. K.; Ferrari, A. C. Raman Fingerprint of Charged Impurities in Graphene. *Appl. Phys. Lett.* **2007**, *91*, 233108.

(10) Ni, Z. H.; Yu, T.; Luo, Z. Q.; Wang, Y. Y.; Liu, L.; Wong, C. P.; Miao, J.; Huang, W.; Shen, Z. X. Probing Charged Impurities in Suspended Graphene Using Raman Spectroscopy. *ACS Nano* **2009**, *3*, 569−574.

(11) Pisana, S.; Lazzeri, M.; Casiraghi, C.; Novoselov, K. S.; Geim, A. K.; Ferrari, A. C.; Mauri, F. Breakdown of the Adiabatic Born-Oppenheimer Approximation in Graphene. *Nat. Mater.* **2007**, *6*, 198−201.

(12) Calizo, I.; Bao, W.; Miao, F.; Lau, C. N.; Balandin, A. A. The Effect of Substrates on the Raman Spectrum of Graphene: Graphene-on-Sapphire and Graphene-on-Glass. *Appl. Phys. Lett.* **2007**, *91*, 201904−201903.

(13) Das, A.; Pisana, S.; Chakraborty, B.; Piscanec, S.; Saha, S. K.; Waghmare, U. V.; Novoselov, K. S.; Krishnamurthy, H. R.; Geim, A. K.; Ferrari, A. C.; et al. Monitoring Dopants by Raman Scattering in an Electrochemically Top-Gated Graphene Transistor. *Nat. Nanotechnol.* **2008**, *3*, 210−215.

(14) Das, A.; Chakraborty, B.; Piscanec, S.; Pisana, S.; Sood, A. K.; Ferrari, A. C. Phonon Renormalization in Doped Bilayer Graphene. *Phys. Rev. B* **2009**, *79*, 155417.

DOI: 10.1021/jz5027272
J. Phys. Chem. Lett. 2015, 6, 964−969

(15) Poncharal, P.; Ayari, A.; Michel, T.; Sauvajol, J. L. Raman Spectra of Misoriented Bilayer Graphene. *Phys. Rev. B* **2008**, *78*, 113407.
(16) Sojoudi, H.; Baltazar, J.; Tolbert, L. M.; Henderson, C. L.; Graham, S. Creating Graphene P−N Junctions Using Self-Assembled Monolayers. *ACS Appl. Mater. Interfaces* **2012**, *4*, 4781−4786.
(17) Malard, L. M.; Guimarães, M. H. D.; Mafra, D. L.; Mazzoni, M. S. C.; Jorio, A. Group-Theory Analysis of Electrons and Phonons in N-Layer Graphene Systems. *Phys. Rev. B* **2009**, *79*, 125426.
(18) Dresselhaus, M. S.; Jorio, A.; Hofmann, M.; Dresselhaus, G.; Saito, R. Perspectives on Carbon Nanotubes and Graphene Raman Spectroscopy. *Nano Lett.* **2010**, *10*, 751−758.
(19) Jorio, A.; Ferreira, E. H. M.; Moutinho, M. V. O.; Stavale, F.; Achete, C. A.; Capaz, R. B. Measuring Disorder in Graphene with the G and D Bands. *Phys. Status Solidi B* **2010**, *247*, 2980−2982.
(20) Lucchese, M. M.; Stavale, F.; Ferreira, E. H. M.; Vilani, C.; Moutinho, M. V. O.; Capaz, R. B.; Achete, C. A.; Jorio, A. Quantifying Ion-Induced Defects and Raman Relaxation Length in Graphene. *Carbon* **2010**, *48*, 1592−1597.
(21) You, Y.; Ni, Z.; Yu, T.; Shen, Z. Edge Chirality Determination of Graphene by Raman Spectroscopy. *Appl. Phys. Lett.* **2008**, *93*, 163112−163113.
(22) Casiraghi, C.; Hartschuh, A.; Qian, H.; Piscanec, S.; Georgi, C.; Fasoli, A.; Novoselov, K. S.; Basko, D. M.; Ferrari, A. C. Raman Spectroscopy of Graphene Edges. *Nano Lett.* **2009**, *9*, 1433−1441.
(23) Mohiuddin, T. M. G.; Lombardo, A.; Nair, R. R.; Bonetti, A.; Savini, G.; Jalil, R.; Bonini, N.; Basko, D. M.; Galiotis, C.; Marzari, N.; et al. Uniaxial Strain in Graphene by Raman Spectroscopy: G Peak Splitting Grüneisen Parameters and Sample Orientation. *Phys. Rev. B* **2009**, *79*, 205433.
(24) Ni, Z. H.; Wang, H. M.; Ma, Y.; Kasim, J.; Wu, Y. H.; Shen, Z. X. Tunable Stress and Controlled Thickness Modification in Graphene by Annealing. *ACS Nano* **2008**, *2*, 1033−1039.
(25) Ni, Z. H.; Yu, T.; Lu, Y. H.; Wang, Y. Y.; Feng, Y. P.; Shen, Z. X. Uniaxial Strain on Graphene: Raman Spectroscopy Study and Band-Gap Opening. *ACS Nano* **2008**, *2*, 2301−2305.
(26) Calizo, I.; Balandin, A. A.; Bao, W.; Miao, F.; Lau, C. N. Temperature Dependence of the Raman Spectra of Graphene and Graphene Multilayers. *Nano Lett.* **2007**, *7*, 2645−2649.
(27) Dresselhaus, M. S.; Jorio, A.; Saito, R. Characterizing Graphene Graphite and Carbon Nanotubes by Raman Spectroscopy. *Annu. Rev. Condens. Matter Phys.* **2010**, *1*, 89−108.
(28) Ferrari, A. C.; Meyer, J. C.; Scardaci, V.; Casiraghi, C.; Lazzeri, M.; Mauri, F.; Piscanec, S.; Jiang, D.; Novoselov, K. S.; Roth, S.; et al. Raman Spectrum of Graphene and Graphene Layers. *Phys. Rev. Lett.* **2006**, *97*, 187401.
(29) Malard, L. M.; Pimenta, M. A.; Dresselhaus, G.; Dresselhaus, M. S. Raman Spectroscopy in Graphene. *Phys. Rep.* **2009**, *473*, 51−87.
(30) Tang, B.; Guoxin, H.; Gao, H. Raman Spectroscopic Characterization of Graphene. *Appl. Spectrosc. Rev.* **2010**, *45*, 369−407.
(31) Ferrari, A. C. Raman Spectroscopy of Graphene and Graphite: Disorder Electron−Phonon Coupling Doping and Nonadiabatic Effects. *Solid State Commun.* **2007**, *143*, 47−57.
(32) Tuinstra, F.; Koenig, J. L. Raman Spectrum of Graphite. *J. Chem. Phys.* **1970**, *53*, 1126−1130.
(33) Ferrari, A. C.; Robertson, J. Interpretation of Raman Spectra of Disordered and Amorphous Carbon. *Phys. Rev. B* **2000**, *61*, 14095−14107.
(34) Banhart, F.; Kotakoski, J.; Krasheninnikov, A. V. Structural Defects in Graphene. *ACS Nano* **2010**, *5*, 26−41.
(35) Hashimoto, A.; Suenaga, K.; Gloter, A.; Urita, K.; Iijima, S. Direct Evidence for Atomic Defects in Graphene Layers. *Nature* **2004**, *430*, 870−873.
(36) Meyer, J. C.; Kisielowski, C.; Erni, R.; Rossell, M. D.; Crommie, M. F.; Zettl, A. Direct Imaging of Lattice Atoms and Topological Defects in Graphene Membranes. *Nano Lett.* **2008**, *8*, 3582−3586.
(37) Ma, J.; Alfè, D.; Michaelides, A.; Wang, E. Stone-Wales Defects in Graphene and Other Planar Sp^2-Bonded Materials. *Phys. Rev. B* **2009**, *80*, 033407.
(38) Lee, G.-D.; Wang, C. Z.; Yoon, E.; Hwang, N.-M.; Kim, D.-Y.; Ho, K. M. Diffusion Coalescence and Reconstruction of Vacancy Defects in Graphene Layers. *Phys. Rev. Lett.* **2005**, *95*, 205501.
(39) Araujo, P. T.; Mauricio, T.; Dresselhaus, M. S. Defects and Impurities in Graphene-Like Materials. *Mater. Today* **2012**, *15*, 98−109.
(40) Yazyev, O. V.; Tavernelli, I.; Rothlisberger, U.; Helm, L. Early Stages of Radiation Damage in Graphite and Carbon Nanostructures: A First-Principles Molecular Dynamics Study. *Phys. Rev. B* **2007**, *75*, 115418.
(41) Yoon, M.; Han, S.; Kim, G.; Lee, S. B.; Berber, S.; Osawa, E.; Ihm, J.; Terrones, M.; Banhart, F.; Charlier, J.-C.; et al. Zipper Mechanism of Nanotube Fusion: Theory and Experiment. *Phys. Rev. Lett.* **2004**, *92*, 075504.
(42) Kim, Y.-H.; Lee, I.-H.; Chang, K. J.; Lee, S. Dynamics of Fullerene Coalescence. *Phys. Rev. Lett.* **2003**, *90*, 065501.
(43) Sammalkorpi, M.; Krasheninnikov, A.; Kuronen, A.; Nordlund, K.; Kaski, K. Mechanical Properties of Carbon Nanotubes with Vacancies and Related Defects. *Phys. Rev. B* **2004**, *70*, 245416.
(44) Duplock, E. J.; Scheffler, M.; Lindan, P. J. D. Hallmark of Perfect Graphene. *Phys. Rev. Lett.* **2004**, *92*, 225502.
(45) OuYang, F.; Huang, B.; Li, Z.; Xiao, J.; Wang, H.; Xu, H. Chemical Functionalization of Graphene Nanoribbons by Carboxyl Groups on Stone-Wales Defects. *J. Phys. Chem. C* **2008**, *112*, 12003−12007.
(46) Stone, A. J.; Wales, D. J. Theoretical Studies of Icosahedral C_{60} and Some Related Species. *Chem. Phys. Lett.* **1986**, *128*, 501−503.
(47) Suenaga, K.; Wakabayashi, H.; Koshino, M.; Sato, Y.; Urita, K.; Iijima, S. Imaging Active Topological Defects in Carbon Nanotubes. *Nat. Nanotechnol.* **2007**, *2*, 358−360.
(48) Kotakoski, J.; Meyer, J. C.; Kurasch, S.; Santos-Cottin, D.; Kaiser, U.; Krasheninnikov, A. V. Stone-Wales-Type Transformations in Carbon Nanostructures Driven by Electron Irradiation. *Phys. Rev. B* **2011**, *83*, 245420.
(49) Kotakoski, J.; Krasheninnikov, A. V.; Kaiser, U.; Meyer, J. C. From Point Defects in Graphene to Two-Dimensional Amorphous Carbon. *Phys. Rev. Lett.* **2011**, *106*, 105505.
(50) El-Barbary, A. A.; Telling, R. H.; Ewels, C. P.; Heggie, M. I.; Briddon, P. R. Structure and Energetics of the Vacancy in Graphite. *Phys. Rev. B* **2003**, *68*, 144107.
(51) Krasheninnikov, A. V.; Nordlund, K.; Sirviö, M.; Salonen, E.; Keinonen, J. Formation of Ion-Irradiation-Induced Atomic-Scale Defects on Walls of Carbon Nanotubes. *Phys. Rev. B* **2001**, *63*, 245405.
(52) Kaxiras, E.; Pandey, K. C. Energetics of Defects and Diffusion Mechanisms in Graphite. *Phys. Rev. Lett.* **1988**, *61*, 2693−2696.
(53) Schalnat, M. C.; Hawkridge, A. M.; Pemberton, J. E. Raman Spectroscopy of the Reaction of Thin Films of Solid-State Benzene with Vapor Deposited Ag Mg and Al. *J. Phys. Chem. C* **2011**, *115*, 13717−13724.
(54) Matz, D. L.; Ratcliff, E. L.; Meyer, J.; Kahn, A.; Pemberton, J. E. Deciphering the Metal-C_{60} Interface in Optoelectronic Devices: Evidence for C_{60} Reduction by Vapor Deposited Al. *ACS Appl. Mater. Interfaces* **2013**, *5*, 6001−6008.
(55) Matz, D. L.; Pemberton, J. E. Reaction Chemistry of Solid-State Pyridine Thin Films with Vapor Deposited Ag Mg and Al. *J. Phys. Chem. C* **2012**, *116*, 11548−11555.
(56) Davis, R. J.; Pemberton, J. E. Investigation of the Interfaces of Tris-(8-Hydroxyquinoline) Aluminum with Ag and Al Using Surface Raman Spectroscopy. *J. Phys. Chem. C* **2008**, *112*, 4364−4371.
(57) Tiani, D. J.; Pemberton, J. E. Emersion of 11-Mercapto-1-Undecanol-Modified Ag Substrates from Aqueous and Nonaqueous Solvents: The Effect of Emersion Velocity on Emersed Solvent Layer Thickness. *Langmuir* **2003**, *19*, 6422−6429.
(58) Taylor, C. E.; Garvey, S. D.; Pemberton, J. E. Carbon Contamination at Silver Surfaces: Surface Preparation Procedures Evaluated by Raman Spectroscopy and X-Ray Photoelectron Spectroscopy. *Anal. Chem.* **1996**, *68*, 2401−2408.
(59) Taylor, C. E.; Pemberton, J. E.; Goodman, G. G.; Schoenfisch, M. H. Surface Enhancement Factors for Ag and Au Surfaces Relative

DOI: 10.1021/jz5027272
J. Phys. Chem. Lett. 2015, 6, 964−969

to Pt Surfaces for Monolayers of Thiophenol. *Appl. Spectrosc.* **1999**, *53*, 1212−1221.
(60) Hawkridge, A. M.; Pemberton, J. E. Model Aluminum-Poly(P-Phenylenevinylene) Interfaces Studied by Surface Raman Spectroscopy. *J. Am. Chem. Soc.* **2002**, *125*, 624−625.
(61) Teweldebrhan, D.; Balandin, A. A. Modification of Graphene Properties Due to Electron-Beam Irradiation. *Appl. Phys. Lett.* **2009**, *94*, 013101.
(62) Liu, G.; Teweldebrhan, D.; Balandin, A. A. Tuning of Graphene Properties Via Controlled Exposure to Electron Beams. *IEEE Trans. Nanotechnol.* **2011**, *10*, 865−870.
(63) Zhou, Z.; Gao, F.; Goodman, D. W. Deposition of Metal Clusters on Single-Layer Graphene/Ru(0001): Factors That Govern Cluster Growth. *Surf. Sci.* **2010**, *604*, L31−L38.
(64) Zhou, H.; Qiu, C.; Yu, F.; Yang, H.; Chen, M.; Hu, L.; Sun, L. Thickness-Dependent Morphologies and Surface-Enhanced Raman Scattering of Ag Deposited on N-Layer Graphenes. *J. Phys. Chem. C* **2011**, *115*, 11348−11354.
(65) Lin, H.-Y.; Hung, M.-L.; Huang, C.-H.; Chui, H.-C.; Lin, J.-S. Graphene Layer Number Dependent Size Distribution of Silver Nanoparticles. *Appl. Phys. A: Mater. Sci. Process.* **2014**, *115*, 399−402.
(66) Huang, C.-W.; Lin, H.-Y.; Huang, C.-H.; Shiue, R.-J.; Wang, W.-H.; Liu, C.-Y.; Chui, H.-C. Layer-Dependent Morphologies of Silver on N-Layer Graphene. *Nanoscale Res. Lett.* **2012**, *7*, 618.
(67) Ramasse, Q. M.; Zan, R.; Bangert, U.; Boukhvalov, D. W.; Son, Y.-W.; Novoselov, K. S. Direct Experimental Evidence of Metal-Mediated Etching of Suspended Graphene. *ACS Nano* **2012**, *6*, 4063−4071.
(68) Rodríguez-Manzo, J. A.; Cretu, O.; Banhart, F. Trapping of Metal Atoms in Vacancies of Carbon Nanotubes and Graphene. *ACS Nano* **2010**, *4*, 3422−3428.
(69) Srivastava, M. K.; Wang, Y.; Kemper, A. F.; Cheng, H.-P. Density Functional Study of Gold and Iron Clusters on Perfect and Defected Graphene. *Phys. Rev. B* **2012**, *85*, 165444.
(70) Lim, D.-H.; Negreira, A. S.; Wilcox, J. Dft Studies on the Interaction of Defective Graphene-Supported Fe and Al Nanoparticles. *J. Phys. Chem. C* **2011**, *115*, 8961−8970.
(71) Santos, J. E.; Peres, N. M. R.; Lopes dos Santos, J. M. B.; Castro Neto, A. H. Electronic Doping of Graphene by Deposited Transition Metal Atoms. *Phys. Rev. B* **2011**, *84*, 085430.
(72) Okamoto, Y. Density-Functional Calculations of Icosahedral M_{13} (M = Pt and Au) Clusters on Graphene Sheets and Flakes. *Chem. Phys. Lett.* **2006**, *420*, 382−386.
(73) Stiles, P. L.; Dieringer, J. A.; Shah, N. C.; Van Duyne, R. P. Surface-Enhanced Raman Spectroscopy. *Annu. Rev. Anal. Chem.* **2008**, *1*, 601−626.
(74) Xu, W.; Ling, X.; Xiao, J.; Dresselhaus, M. S.; Kong, J.; Xu, H.; Liu, Z.; Zhang, J. Surface Enhanced Raman Spectroscopy on a Flat Graphene Surface. *Proc. Natl. Acad. Sci. U. S. A.* **2012**, *109*, 9281−9286.
(75) Zhong, L.-B.; Yin, J.; Zheng, Y.-M.; Liu, Q.; Cheng, X.-X.; Luo, F.-H. Self-Assembly of Au Nanoparticles on Pmma Template as Flexible, Transparent, and Highly Active Sers Substrates. *Anal. Chem.* **2014**, *86*, 6262−6267.
(76) Jiao, L.; Fan, B.; Xian, X.; Wu, Z.; Zhang, J.; Liu, Z. Creation of Nanostructures with Poly(Methyl Methacrylate)-Mediated Nanotransfer Printing. *J. Am. Chem. Soc.* **2008**, *130*, 12612−12613.
(77) Kudin, K. N.; Ozbas, B.; Schniepp, H. C.; Prud'homme, R. K.; Aksay, I. A.; Car, R. Raman Spectra of Graphite Oxide and Functionalized Graphene Sheets. *Nano Lett.* **2007**, *8*, 36−41.
(78) Li, L.; Reich, S.; Robertson, J. Defect Energies of Graphite: Density-Functional Calculations. *Phys. Rev. B* **2005**, *72*, 184109.
(79) Severin, N.; Kirstein, S.; Sokolov, I. M.; Rabe, J. P. Rapid Trench Channeling of Graphenes with Catalytic Silver Nanoparticles. *Nano Lett.* **2009**, *9*, 457−461.
(80) Booth, T. J.; Pizzocchero, F.; Andersen, H.; Hansen, T. W.; Wagner, J. B.; Jinschek, J. R.; Dunin-Borkowski, R. E.; Hansen, O.; Bøggild, P. Discrete Dynamics of Nanoparticle Channelling in Suspended Graphene. *Nano Lett.* **2011**, *11*, 2689−2692.
(81) Stanghellini, P. L.; Diana, E.; Arrais, A.; Rossin, A.; Kettle, S. F. A. Benzene and Tropilium Metal Complexes. Intra- and Intermolecular Interaction Evidenced by Vibrational Analysis: The Blue-Shift Hydrogen Bond. *Organometallics* **2006**, *25*, 5024−5030.
(82) Dresselhaus, M. S.; Jorio, A.; Cançado, L. G.; Dresselhaus, G.; Saito, R., Raman Spectroscopy: Characterization of Edges Defects and the Fermi Energy of Graphene and sp^2 Carbons. In *Graphene Nanoelectronics*; Raza, H., Ed.; Springer: Berlin, 2012; pp 15−55.

DOI: 10.1021/jz5027272
J. Phys. Chem. Lett. 2015, 6, 964−969